Diffraction enhanced transparency and slow THz light in periodic arrays of detuned and displaced dipoles

Martijn C. Schaafsma [0],[†,‡] Arkabrata Bhattacharya [0],[†,¶] and Jaime Gómez Rivas[*,¶,§]

†*Center for Nanophotonics, FOM Institute AMOLF, P.O. Box 41883, 1009 DB Amsterdam, The Netherlands*

‡*Current address: Bright Society, High Tech Campus 68, 5656 AG Eindhoven, The Netherlands*

¶*Dutch Institute for Fundamental Energy Research, DIFFER, P.O. Box 6336, 5600 HH Eindhoven, The Netherlands*

§*Cobra Research Institute, Eindhoven University of Technology, P.O. Box 513, 5600 MB Eindhoven The Netherlands*

E-mail: j.gomezrivas@differ.nl

Phone: +31-20-754-7100. Fax: +31-20-754-7290

Abstract

We demonstrate that a periodic lattice of detuned resonators can suppress the THz extinction at the central resonant frequency, leading to an enhanced transparency due to diffraction. The system consists of metallic rods of two different sizes, each of them supporting a strong half-wavelength ($\lambda/2$) resonance, which are spatially displaced

[0]M. C. Schaafsma and A. Bhattacharya contributed equally to this work.

within the unit cell of the lattice. Using a coupled dipole model we show that the Diffraction Enhanced Transparency (DET) window has its origin in the interference between two surface lattice resonances, arising from the diffractively enhanced radiative coupling of the $\lambda/2$ resonances in the lattice. Group-index measurements show that the THz field is strongly delayed by more than four orders of magnitude at the transparency window. Since DET does not involve the near-field coupling of resonators, the fabrication tolerance to imperfections is expected to be very high. This remarkable response renders these systems as very interesting components for THz communication.

Keywords

surface lattice resonance, electromagnetically induced transparency, terahertz transmission, coupled dipole model

Small metallic particles are among the simplest electromagnetic resonators. The resonances in these scatterers depend on the particle size, shape, orientation and material,[1] and are usually broad due to radiative losses.[2] Ensembles of scatterers have properties that depend on the individual scatterers, as well as their relative arrangement. For instance, bringing two metallic nanoparticles close together in dimer[3–5] or more elaborate[6] configurations can have a significant effect on the resonance frequency. An important recent development in nanophotonics involves the generation of transparency windows induced by coupling of electromagnetic resonances.[7–9] This phenomenon usually involves a bright (dipolar) resonance that can couple to the radiation field and a dark (multipolar) resonance that couples to the bright resonance through its near field.[8] The coupling and interference of the two resonances leads to a frequency window in which the transmission is close to unity, while local fields are enhanced.[10,11] These transparency windows are analogous to the electromagnetically induced transparencies (EIT) observed in atomic systems coupled to light fields.[12] The most important characteristic of these systems is that they can slow light to extremely low group velocities while having a transmission close to unity. Bozhevolnyi and coworkers have re-

cently demonstrated the existence of a transparency window in the transmission spectrum of a system of two coupled particles of different dimensions, such that their dipolar resonant frequencies are detuned from each other at optical frequencies.[13–15] The mechanism leading to this transparency window is the radiative coupling between the two resonators and the destructive interference of the electromagnetic fields radiated into the far-field, and can be described as a coupled resonator induced transparency.[16,17] Other examples include resonators coupled to a waveguide,[18,19] coupled microcavities[20] and ring resonators.[21]

In this article, we demonstrate a spectral transparency window at THz frequencies with nearly perfect transmission in a periodic lattice of metallic rods with different dimensions. In contrast to previous works on detuned resonant particles,[13–15] we consider here a periodic lattice of detuned resonators, which supports surface lattice resonances (SLRs). These resonances are the result of the enhanced radiative coupling of the localized resonances in the individual particles through diffraction orders in the plane of the array (Rayleigh Anomalies).[22–33] Periodic arrays of detuned dipoles have been recently considered by Humphrey et. al. as a means to reduce the line-width of surface lattice resonances.[34] Our experimental results show a highly enhanced group-index, i.e., reduced group velocities, in the transparency window. Since the periodic arrangement of particles are responsible for the enhanced transparency of the sample, we term this phenomenon as diffraction enhanced transparency (DET). These results are explained with a coupled dipole model, which describes the system as interfering SLRs. Slow THz light has been reported in several works.[35–38] In contrast to these works, our system of detuned-dipoles shows a simple approach to engineer frequency selective transparency windows with very large transmission and group velocity reduction. The group velocity reduction is significantly larger than in plasmonic induced transparency systems.[7,8,39] The enhanced reduction of group velocity is a result of DET not relying on near-field coupling, but on the interference of surface waves, as shown in the manuscript. These remarkable properties make these arrays interesting components for the emerging field of THz communication.

Sample design and measurements

Using optical lithography, metal deposition and lift-off, we have fabricated samples containing 2D periodic lattices of gold rods on top of a 3 mm thick amorphous quartz substrate. Before the thermal evaporation of the 100 nm gold layer a 2 nm chromium adhesion layer was deposited.

Figure 1(a) shows an optical microscope image of the periodic lattice of detuned resonators. This sample consists of two gold rods with different sizes per unit cell of the lattice. The dimensions of the rods are 200 μm × 40 μm and 125 μm × 60 μm, and are referred to as the 'long' and 'short' rods, respectively. Both type of rods support resonances when illuminated with THz radiation, however the resonant frequencies are detuned from each other due to the different dimensions. Note that the width of the short rods in Figure 1(a) is larger than that of the long rods, which ensures a similar volume and surface coverage for the two types of rods. The lattice has a square symmetry with a period of 300 μm in both directions. The separation between the detuned resonators is 150 μm along the short axis of the rods.

A similar sample was prepared in which the short rods were replaced by the long rods in each unit cell. An optical microscope image of this sample is shown in Figure 1(b). We refer to this sample as the array of identical resonators. Two other samples are shown in Figures 1(c) and 1(d). These samples represent the periodic arrays of the individual long and short rods in each unit cell respectively. The periodicity of all the samples is the same as in the array of detuned resonators. The samples shown in Figure 1(b), (c) and (d) are control samples to understand the underlying mechanism of DET in the sample of the detuned resonators. To study the effect of periodicity on the response of these samples we have also made samples where each of the detuned, identical, long and short resonators respectively are randomly distributed over the substrate. (See images in the supporting information.)

The experiments were carried out using a THz time domain spectrometer. In this setup a train of femtosecond pulses with a central wavelength of 800 nm from an Ti:Sapphire

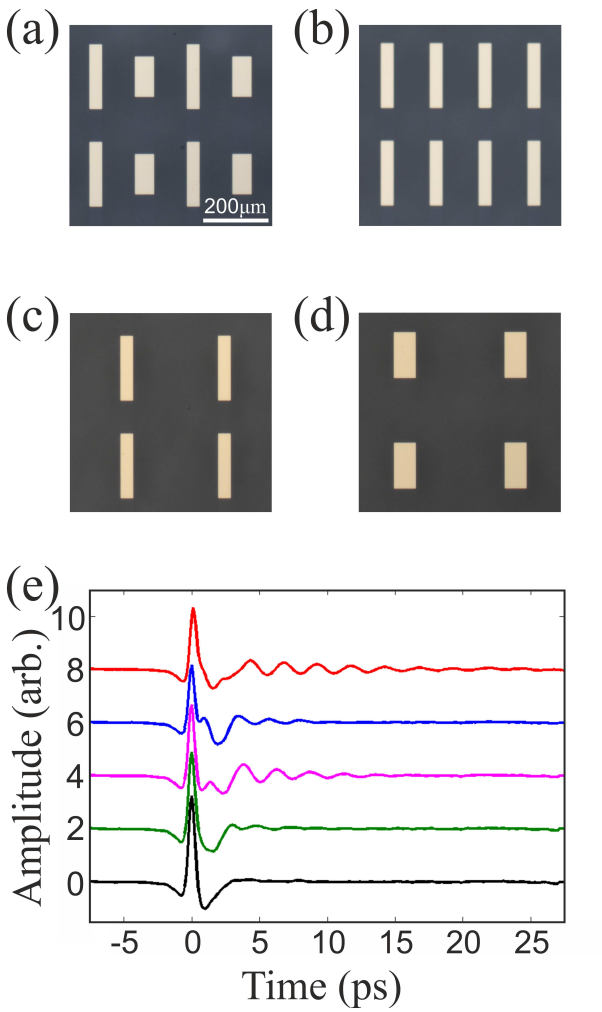

Figure 1: Optical microscope images of square periodic arrays of (a) detuned, (b) identical, (c) long and (d) short gold rods defining THz resonators with a period of 300 μm on top of a quartz substrate. The dimensions of the long rods are 200 μm × 40 μm, and those of the short rods are 125 μm × 60 μm. (e) THz transients of the forward transmission measured for the periodic arrays of detuned (red curve), identical (blue curve) long (magenta curve) and short (green curve) rods respectively, as well as the reference (black curve) measured through a quartz substrate without rods are shown. The transients are displaced vertically for clarity.

oscillator is split in two beams that are respectively used for the generation and detection of broadband single-cycle THz pulses. For the generation we use a biased photoconductive antenna that is switched on by the pulses from one of the 800 nm optical beams. The THz pulses, after transmission through the sample, are detected with a second photoconductive antenna that it is gated by the pulses from the other optical beam. By controlling the time delay between the generation and detection optical pulses, the spectrometer measures the transmitted THz electric field amplitude as a function of this time delay. The numerical aperture of the collection lens is $\sim$0.34. This guarantees that it collects only the zeroth order transmission for frequencies below 1.5 THz.

Figure 1(e) displays the transients of the THz transmission in the forward direction through the periodic arrays containing the detuned (red curve), the identical (blue curve), the individual long (magenta) and the individual short (green) resonators. The polarization of the THz electromagnetic field is set parallel to the long axes of the rods, and the THz beam propagates at normal incidence through the sample. The black curve in Figure 1(e) corresponds to a reference measurement taken through a quartz substrate without any rods. This reference shows the single-cycle THz pulse. The thickness of 3 mm of the substrate leads to a first reflection which is delayed by 40 ps with respect to the main THz pulse, i.e., outside the time window of the measurements. The transient measured through the array of identical resonators shows some oscillations (blue curve in Fig. 1(e)) after the main peak. For the long resonators, the oscillations (the magenta curve in Fig. 1(e)) extend to later times up to around 12 ps and for the array of shorter resonators the oscillations (the green curve in Fig. 1(e)) vanish within 6-7 ps. The main peaks in the transients at 0 ps correspond to the fraction of the THz amplitude that it is not scattered or absorbed by the array. The rapid vanishing of the THz amplitude is an indication of a limited resonant interaction of the THz pulse with the array. The THz transient of the transmission through array of detuned resonators is pronouncedly different although the metal filling fractions of both samples are very similar. For the array of detuned resonators we observe that the

THz transient contains a harmonic damped oscillation (red curve in Fig. 1(e)) which extends up to 25 ps. Such strong dispersion due to a periodic system is a characteristic behavior of diffraction enhanced transparency (DET). The harmonic THz signal at long time delays indicates the reduction of the group velocity in a narrow frequency window, as we show next.

The THz transients can be Fourier transformed to obtain the extinction of the arrays and the phase spectra of the transmitted signal. The complex transmitted field through the sample of detuned resonators can be written as $E(\nu)\exp(i\phi'(\nu))$, where $E(\nu)$ is the transmitted amplitude and $\phi'(\nu)$ the phase. The transmitted field through the bare substrate is given by $E_{ref}(\nu)\exp(i\phi_{ref}(\nu))$. The resulting amplitude transmission can be expressed as

$$t = \frac{E(\nu)e^{i\phi'(\nu)}}{E_{ref}(\nu)e^{i\phi_{ref}(\nu)}} = \frac{E(\nu)}{E_{ref}(\nu)}e^{i\Delta\phi(\nu)} , \tag{1}$$

where $\Delta\phi(\nu) = \phi'(\nu) - \phi_{ref}(\nu)$ is the phase delay spectrum. We define the THz extinction spectra of the samples as

$$\mathcal{S} = 1 - |t|^2 . \tag{2}$$

The extinction spectra are shown in Figure 2(a), where the blue curve corresponds to the extinction of the array of identical resonators and the red curve to the extinction of the arrays of detuned resonators. The former is characterized by a broad resonance with a maximum extinction at 0.45 THz. This resonance in the extinction corresponds to the resonant absorption and mainly to the resonant scattering of the $\lambda/2$ resonance along the long axis of the rods. The THz electric field drives an electrical current along this axis that resonates over the length of the rods at this particular frequency. Note, that the resonance wavelength (667 μm) is longer than 2 times of the physical length of the rods, which can be attributed to the presence of the quartz substrate, the impedance at the edges of the rods,[40] and diffractive coupling with the other rods in the array. The extinction spectrum changes drastically when one of the rods in the unit cell is replaced by the shorter one (red

open circles in figure 2(a)). A window in which the extinction vanishes (the DET window) appears at 0.45 THz, and an additional maximum in the extinction appears at 0.4 THz. The vanishing extinction corresponds to a nearly full transmission at this particular frequency (Transmission = 99.2 ± 0.5 %). In the next section we show, using a coupled dipole model, that the DET window is the result of the interference of surface lattice resonances in the array of detuned resonators. The period of the lattice, which plays a crucial role, was chosen such that the DET is the largest in the frequency range of maximum sensitivity of the THz spectrometer. The importance of the lattice constant is illustrated in Fig. S3 of the Supporting Information.

The frequency-dependent phase delay, $\Delta\phi(\nu)$, obtained from the Fourier transform of the THz pulses transmitted through the arrays are displayed on Fig. 2(b). The phase delay for the array of identical resonators (blue open squares) presents the characteristic dispersion of a damped oscillator, with a change of sign in the phase at the resonant frequency of maximum extinction (marked by the vertical dashed line in the figure). The phase delay dispersion for the array of detuned oscillators (red open circles in Figure 2(b)) is pronouncedly different. The phase changes sign at the frequency of maximum extinction, but recovers its positive values at the transparency frequency (marked with the dashed line in the figure), where the system is highly dispersive in spite of the vanishing extinction. The phase delay, as defined earlier, can be written as,

$$\Delta\phi(\nu) = \phi'(\nu) - \phi_{ref}(\nu) = (\phi(\nu) + \phi_{quartz}(\nu)) - (\phi_0(\nu) + \phi_{quartz}(\nu)), \tag{3}$$

where, $\phi(\nu)$ is the phase introduced solely by the array of the detuned resonators, $\phi_{quartz}(\nu)$ is the phase introduced by the quartz substrate (which is the same for sample and the reference) and $\phi_0(\nu)$ is the phase introduced by the layer of air with the same thickness as

the lattice of detuned resonators. Therefore,

$$\Delta\phi(\nu) = (k(\nu) - k_0(\nu))L, \tag{4}$$

where $k(\nu)$ is the wave vector in the array of the detuned dipole and $k_0(\nu) = 2\pi\nu/c$ is the wave vector in air and L is the thickness of the array of resonators. The group index can be determined from the phase delay using the following expression [41,42]

$$n_g(\nu) = \frac{c_0}{v_g(\nu)} = c_0\frac{dk(\nu)}{d\nu} = \frac{c_0}{L}\frac{d\Delta\phi(\nu)}{d\nu} + 1\ , \tag{5}$$

where c_0 is the speed of light in vacuum and $v_g(\nu)$ is the group velocity, and phases are in units of 2π radians. In figure 2(c) we plot the dependence of the group index on the frequency for both arrays of detuned (red open circles) and identical (blue open circles) resonators. The group index has a maximum value of more than 6×10^4 for the array of detuned resonators. This remarkably large change in group index, corresponds to a group velocity of 5×10^3 m/s at 0.45 THz, i.e., at the frequency of full transmission. At this frequency the wave is delayed by scattering within the array and is re-radiated in the forward direction. In comparison, it can be seen that no such dramatic increase in the group index is observed for the array of identical dipoles.

We have performed more measurements to elucidate the mechanism of such a unique spectral behavior. First, we have measured a random array of the detuned resonators to illustrate the influence of the periodic array on the DET. We see from Figure 3(a)(red open circles), that although there is a window of partial reduction of the extinction, it does not reach very low values at that frequency. This indicates that the periodicity in the array of the detuned resonators plays an important role in the DET. The spectral response from the random array of the identical resonators is also shown in Figure 3(a) (blue open squares). The different curves in Fig. 3(b) show the extinction due to the periodic array of the individual long rods (magenta open circles), the periodic array of the individual short rods (green open

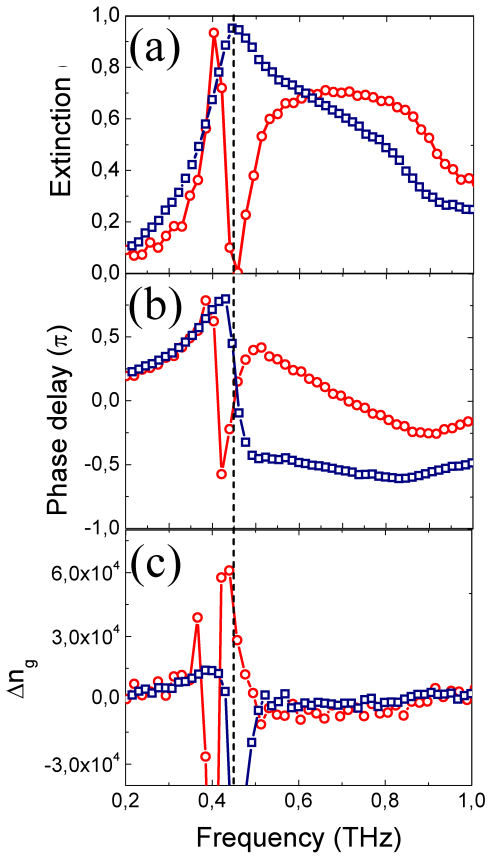

Figure 2: Extinction (a), phase delay (b), and group index (c) spectra of the arrays of detuned (red open circles) and identical (blue open squares) resonators corresponding to the transients shown in figure 1(e). The reference sample is an empty quartz substrate. The vertical dotted line at 0.45 THz indicates the frequency of induced transparency for the array with the detuned resonators.

triangles), the random array of the long rods (magenta solid) and the random array of short rods (green dashes). The measurements in random arrays are done to elucidate the spectral responses of the individual rods keeping in mind that the randomness averages out any effect due to diffractive coupling between individual rods. Hence, the extinction of the random arrays of the short and the long rods are proportional to their individual spectral responses. We can appreciate in Fig. 3(b) that the spectral responses of the periodic arrays of both the short and long rods are different from the response of the random arrays of similar rods. This difference is the result of the radiative coupling of the rods. This coupling is enhanced through diffraction in the periodic array. In particular, when the wave-vector of the scattered wave is equal to an integer number times the inverse of the lattice constant of the array, the condition for in-plane diffraction is fulfilled. This condition known as the Rayleigh anomaly, leads to an increased scattered intensity along the plane of the array, which causes an enhanced coupling between the rods. This enhanced coupling is known as surface lattice resonances[24,25,27,31] and gives rise to the red-shift and narrowing of the resonance. Note that the values of the extinctions of the arrays of long and short resonators (Figure 2(a)) do not reach zero around the DET frequency of 0.45 THz. Therefore, the incoherent sum of the two extinctions will never vanish at the DET window. This finite extinction of the arrays of equal resonators supports the interpretation that the response of the array of detuned resonators is the result of the coherent interference of the amplitudes of the two SLRs. The physics behind the formation of SLRs and their interference can be explained by considering the rods as radiatively coupled resonant dipoles. Therefore, in the following section we use the coupled dipole model to elucidate the underlying mechanism of DET.

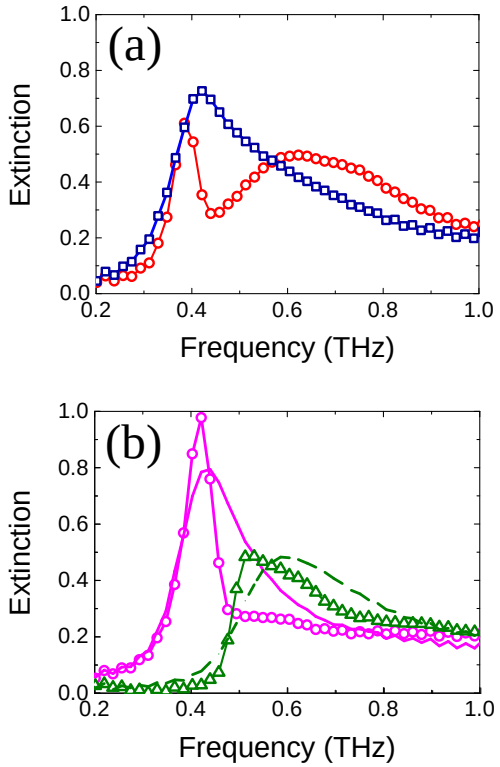

Figure 3: (a) Extinction through a random array of detuned resonators (red open circles) and through a random sample of identical resonators (blue open squares). (b) Extinction through periodic array of individual long rods (magenta open circles), periodic array of individual short rods (green open triangles), random array of individual long rods (magenta solid) and random array of individual short rods (green dashes).

Coupled dipole model

We have used a coupled dipole model to elucidate the underlying mechanism that gives rise to DET. For simplicity we have considered a 1D chain of dipoles embedded in a homogeneous environment with the refractive index of quartz (n=2). These approximations facilitate the interpretation of the results, without reducing their generality.

The extinction cross section of an ensemble of metallic scatterers is related to the amount of work an incident electromagnetic wave does while driving the conducting electrons of these scatterers. This cross section can be expressed in terms of the wavenumber k, the polarization $\mathbf{p}_i$ of the i^{th}-scatterer and the incident field $\mathbf{E}_i^{\text{inc}}$ according to the following equation,[43]

$$C_{\text{ext}} = 4\pi k \sum_i \frac{\text{Im}(\mathbf{E}_i^{\text{inc}} \cdot \mathbf{p}_i)}{|\mathbf{E}_i^{\text{inc}}|^2} \ . \tag{6}$$

The polarization in turn depends on the incident field, the properties of the scatterer like material and shape and, for an ensemble of scatterers, their relative arrangement. The properties of the scatterer are described by the polarizability tensor $\underline{\underline{\alpha}}$ which relates the polarization and the local field as $\mathbf{p}_i = \underline{\underline{\alpha_i}} \mathbf{E}_i^{\text{loc}}$. In an ensemble of scatterers the local field at each scatterer i is the sum of the incident field, $\mathbf{E}_i^{\text{inc}}$, and the field scattered by all other scatterers, $\mathbf{E}_i^{\text{sca}}$:

$$\mathbf{p}_i = \underline{\underline{\alpha_i}} \mathbf{E}_i^{\text{loc}} = \underline{\underline{\alpha_i}} (\mathbf{E}_i^{\text{inc}} + \mathbf{E}_i^{\text{sca}}) \ . \tag{7}$$

The interaction through scattering between two sub-wavelength scatterers as a function of their respective distance $\mathbf{r}$ can be approximated with the dipole-dipole interaction tensor $\underline{\underline{\text{G}}}(\mathbf{r})$.[44] Considering the sum over all dipoles gives

$$\mathbf{E}_i^{\text{sca}} = \sum_{j \neq i} \underline{\underline{G}}(\mathbf{r}_i - \mathbf{r}_j) \mathbf{p}_j \ . \tag{8}$$

In an infinite periodic lattice that is illuminated by a plane-wave, the behavior of all unit cells is identical over the full array and similar scatterers will have similar polarizations.

When each unit cell contains two -not necessarily similar- scatterers the sum over all dipoles in Eq. (8) can be split in two contributions: one accounting for the interaction with all like dipoles, and the other accounting for the interaction with all unlike dipoles. If we label the dipoles either $\circ$ or $\bullet$, we can express the polarization of Eq. (7) as

$$\mathbf{p}_\circ = \underline{\underline{\alpha}}_\circ \left[\mathbf{E}_\circ^{\text{inc}} + \sum_{j \in \circ} \underline{\underline{G}}_{\circ,j} \mathbf{p}_\circ + \sum_{j \in \bullet} \underline{\underline{G}}_{\circ,j} \mathbf{p}_\bullet \right] , \tag{9}$$

and

$$\mathbf{p}_\bullet = \underline{\underline{\alpha}}_\bullet \left[\mathbf{E}_\bullet^{\text{inc}} + \sum_{j \in \bullet} \underline{\underline{G}}_{\bullet,j} \mathbf{p}_\bullet + \sum_{j \in \circ} \underline{\underline{G}}_{\bullet,j} \mathbf{p}_\circ \right] . \tag{10}$$

Equations (9) and (10) can be re-written in matrix form $\mathbf{E}^{\text{inc}} = M \cdot \mathbf{P}$, where the matrix M accounts for the diffractive coupling. More explicitly,

$$\begin{pmatrix} \mathbf{E}_\circ^{\text{inc}} \\ \mathbf{E}_\bullet^{\text{inc}} \end{pmatrix} = \begin{pmatrix} \underline{\underline{\alpha}}_\circ{}^{-1} - \underline{\underline{S}}_{\circ\circ} & -\underline{\underline{S}}_{\circ\bullet} \\ -\underline{\underline{S}}_{\bullet\circ} & \underline{\underline{\alpha}}_\bullet{}^{-1} - \underline{\underline{S}}_{\bullet\bullet} \end{pmatrix} \begin{pmatrix} \mathbf{p}_\circ \\ \mathbf{p}_\bullet \end{pmatrix} . \tag{11}$$

Each of the $\underline{\underline{S}}$ matrices contains a lattice sum, which is defined as

$$\underline{\underline{S}}_{AB} = \sum_{j \in B} \underline{\underline{G}}_{A,j} \mathbf{p}_B , \tag{12}$$

where A and B correspond to either $\circ$ or $\bullet$.

The dipole interaction tensor takes a simple scalar form, $G(\mathbf{r})$, when a 1D chain of dipoles is considered and the polarization is orthogonal to the direction of the chain. The scalar approximation is justified since, as a result of symmetry, the polarization of the particles is always parallel with the polarization of the incident field. The interaction tensor can be simplified to[45]

$$G(r) = \exp(ikr) \left(\frac{ik}{r^2} - \frac{1}{r^3} + \frac{k^2}{r} \right) , \tag{13}$$

in which r is the distance between the respective dipoles. Solving the above equations for $\mathbf{P}$, and applying Eq. (6), the total extinction cross section of the array can be expressed as

$$C_{\text{ext}} = 4\pi k \text{Im}\left(\frac{2\text{S}_{\circ\bullet} - 2\text{S}_{\circ\circ} + \alpha_{\circ}^{-1} + \alpha_{\bullet}^{-1}}{\text{S}_{\circ\circ}^2 - \text{S}_{\circ\bullet}^2 - (\alpha_{\circ}^{-1} + \alpha_{\bullet}^{-1})\text{S}_{\circ\circ} + \alpha_{\circ}^{-1}\alpha_{\bullet}^{-1}}\right) . \tag{14}$$

The periodic array of the long rods is a limiting case of this equation in which we have $\alpha_{\bullet} = 0$. In this case Eq. 14 is reduced to

$$C_{\circ} = 4\pi k \text{Im}\left(\frac{1}{\alpha_{\circ}^{-1} - \text{S}_{\circ\circ}}\right) . \tag{15}$$

For the calculations the rods are approximated as perfect electric conductors, i.e., the permittivity of the metal is $-\infty$. The polarizability of the particles is calculated assuming that they have an ellipsoidal shape[46] and using the modified long wavelength approximation described in Ref. [43], which accounts for a finite size dynamic polarization and radiative damping. This results in

$$\alpha_{\circ} = \frac{1}{\frac{3F}{V} - \frac{2}{3}ik^3 - \frac{2k^2}{d}} , \tag{16}$$

where V is the volume, d the length and F the form factor of the rods for a wave vector k. Figure 4(a) shows the calculated extinctions of the periodic array of the long rods (magenta solid curve) and of one individual isolated long rod (magenta dotted curve) as a function of frequency. Diffraction from the lattice modifies the extinction spectrum of the localized resonance, with a reduction at the Rayleigh anomaly frequency and an enhancement at lower frequency, which leads to a narrowing of extinction spectrum. This is the characteristic line shape of surface lattice resonances. Figure 4(b) shows the lattice sum of the array of the long rods (black curve) as well the inverse polarizibility (magenta curve) of the individual long rods. The frequency of maximum extinction is indicated with the vertical dashed line in the figure, and it occurs when $\alpha_{\circ}^{-1}$ equals $S_{\circ\circ}$, as shown in Figure 4(b). At this frequency the denominator in Eq. 15 vanishes. The dotted line at 0.5 THz corresponds to the frequency

of the Rayleigh anomaly condition, where a diffraction order propagates along the plane of the array. Constructive interference of the scattered amplitudes by the array gives rise to the suppression of extinction in the forward direction at the Rayleigh anomaly, which corresponds to the divergence of the lattice sum, S.

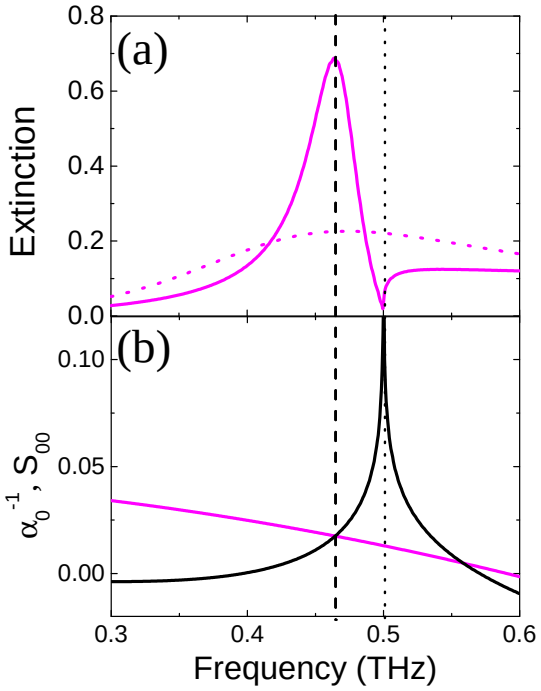

Figure 4: (a) Coupled dipole model calculation of extinction for an 1D array of long rods (magenta solid curve) and a single isolated long rod (magenta dotted curve), and (b) the real components of the lattice sum $S_{\circ\circ}$ and the inverse polarizibility tensor, $\alpha_\circ^{-1}$ of each rod. Both the quantities are in units of inverse volume.

Figure 5(a) displays the calculated spectrum using Eq. 14 for arrays of detuned dipoles with dimensions similar to those used in the experiments. This spectrum shows a sharp resonance with an enhanced extinction followed by a window of diffraction induced transparency at 0.45 THz. This window, indicated by the vertical dotted line in Fig. 5(a), qualitatively reproduces the main characteristics from the experimental response of the detuned dipoles as shown in Fig. 2(a).

The interference of the fields scattered in the plane of the array by the individual lattices of the detuned resonators, indicated by the lattice sum $S_{\circ\bullet}$, is essential for explaining Fig. 5.

If we consider $S_{\circ\bullet} = 0$ in Eq. 14, the equation is reduced to

$$C_{\text{ext}} = 4\pi k \text{Im}\left(\frac{1}{\alpha_{\circ}^{-1} - \text{S}_{\circ\circ}} + \frac{1}{\alpha_{\bullet}^{-1} - \text{S}_{\circ\circ}}\right) = \text{C}_{\circ} + \text{C}_{\bullet}. \tag{17}$$

This expression corresponds to the incoherent sum of the extinctions of the two individual lattices of long and short rods, and is plotted in the Supporting Information in Fig. S2. Both $C_{\circ}$ and $C_{\bullet}$ are SLRs which have finite and positive extinctions for frequencies lower than the Rayleigh anomaly. Therefore, the incoherent sum can not vanish. This situation is represented in the measurements of Fig. 3(b) by the black dotted curve and is distinctly different from the diffraction induced transparency shown by the red open circles in Fig. 2(a). The necessity to include $S_{\circ\bullet}$ in our analysis confirms that DET is the result of the interference of the electromagnetic fields scattered in the plane of the array defined by the lattice sum of equal and unequal scatterers.

Figure 5(b) shows the calculated real components of $S_{\circ\circ}$ (black solid curve), $S_{\circ\bullet}$ (black dashed curve), $\alpha_{\circ}^{-1}$ (magenta curve), and $\alpha_{\bullet}^{-1}$ (green curve). The lattice sums ($S_{\circ\circ}$ and $S_{\circ\bullet}$) diverge at the Rayleigh anomaly condition, i.e. at 0.5 THz, but the corresponding extinction is still finite at this frequency because of their similar values and opposite signs. The opposite signs of the lattice sums can be attributed to the fact that the distances between the like dipoles follow the progression $|\overline{r}| = a, 2a, 3a...$, whereas for the unlike dipoles $|\overline{r}| = \frac{a}{2}, \frac{3a}{2}, \frac{5a}{2}...$, where a is the period of the lattice. Hence, the periodicity is the same for both lattice sums, which explains the divergence at the same frequencies; However, they are out of phase, which explains the opposite signs. The large group index, i.e., low group velocity, described in the previous section with the measurements can be understood by the delay in the wave propagation introduced by scattering into the surface modes of the array. We note that the experimental results do not show a strong reduction of the extinction due to Rayleigh anomalies for single SLRs (open circles and triangles in Fig. 3(b)). This discrepancy with the calculations can be explained by the presence of air-quartz interface in the experiments.

This interface leads to an inhomogeneous surrounding around the particle array. However, the inhomogeneous surrounding does not suppress the DET window introduced by the array of detuned resonators in the measurements, which confirms the robustness of these structures for the realization of induced transparencies.

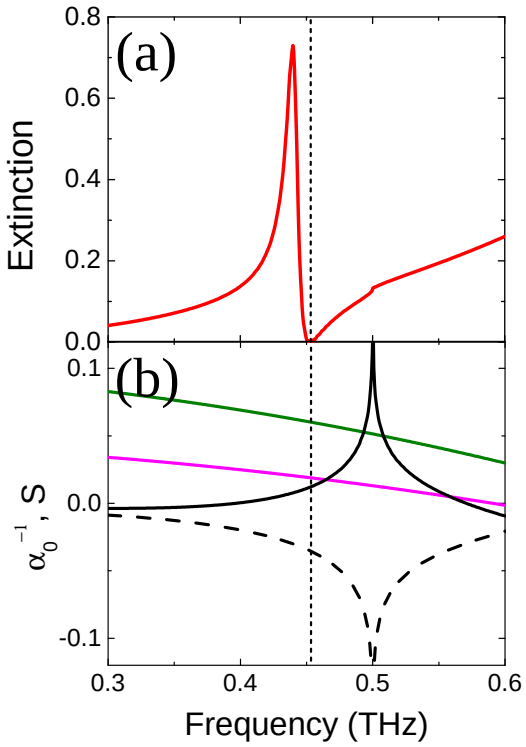

Figure 5: Coupled dipole model calculation for a 1D chain of 2000 unit cells of an array of detuned dipoles. (a) Extinction spectrum (b) real components of $S_{\circ\circ}$ (black solid curve), $S_{\circ\bullet}$ (black dashed curve), $\alpha_{\circ}^{-1}$ (magenta curve) and $\alpha_{\bullet}^{-1}$ (green curve) as presented in Eq. 14.

The dependence of the extinction with displacement between the two detuned dipoles within the unit cell is shown in Fig. 6. Figure 6(a) shows the spectra calculated for three different displacements: 150 μm (red curve), 100 μm (black curve) and 75 μm (blue curve). The curves are vertically offset to elucidate the spectral features with respect to each other. The Rayleigh anomaly, which is represented by the dash-dotted vertical line at 0.5 THz, is fixed for all the calculations. However, for the three different cases the spectral response is very different. By changing the displacement between the two detuned dipoles, it is possible to tune the transparency window in the response of the array. This indicates that even

though the individual SLRs do not change, it is the interference between the two SLRs that is modified due to the relative displacement between the dipoles. Figure 6(b) shows the extinction due to the lattice of detuned dipoles as a function of frequency and displacement between the two dipoles. The three cases shown in Fig. 6(a) are marked by the three horizontal lines at 150, 100 and 75 μm displacement. The Rayleigh anomaly is indicated by the vertical white dash-dotted line at 0.5 THz. The transparency window is symmetric on both sides of the horizontal line at 150 μm where the window is the widest. This is the result of rotational symmetry at this displacement, as the pitch of the array is 300 μm.

In conclusion, we have demonstrated that a periodic array of scatterers with different dimensions can give rise to a narrow spectral transparency window with a transmission close to unity and very large group index. This transparency, which we have termed diffraction enhanced transparency (DET), is the result of the interference of collective resonances known as surface lattice resonances. The surface lattice resonances are the result of the enhanced diffractive coupling of localized resonances in the individual scatterers. The slow wave propagation (the group velocity is reduced by more than 4 orders of magnitude) due to the in-plane scattering and the near perfect transmission, makes DET an interesting phenomenon for the design of components for THz communication, such as modulators or delay elements.

Acknowledgement

The authors thank Gopika Ramanandan, Giorgos Georgiou and Alexei Halpin for valuable discussions and assistance in the experiments. We thank the financial support of ERC through grant no 259272 THZ-PLASMON and the Foundation for Fundamental Research on Matter (FOM), which is part of the Netherlands Organization for Scientific Research (NWO).

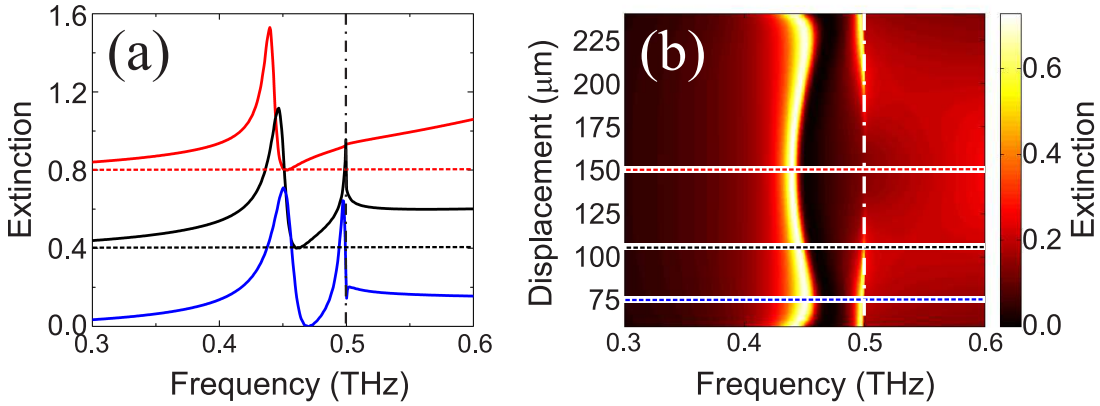

Figure 6: (a) Extinction spectra for two detuned dipoles in a 1D lattice with a pitch of 300 μm. The three cases represents the different displacements between the dipoles; from top, 150 μm (in red), 100 μm (in black) and 75 μm (in blue). The dimensions of the dipoles are the same as before. The spectra are displaced vertically to elucidate the behavior clearly. The dash-dotted vertical line marks the position of the Rayleigh anomaly. (b) Extinction spectra for the lattice of detuned dipoles as a function of frequency and displacements between them. The Rayleigh anomaly condition is indicated by the white dash-dotted vertical line. The three cases shown in (a) is represented by the three horizontal lines at 150, 100 and 75 μm with same color coding.

References

(1) Hutter, E.; Fendler, J. H. Exploitation of localized surface plasmon resonance. *Adv. Mater.* **2004**, *16*, 1685–1706.

(2) Maier, S. A.; Atwater, H. A. Plasmonics: Localization and guiding of electromagnetic energy in metal/dielectric structures. *J. Appl. Phys.* **2005**, *98*, 011101.

(3) Nordlander, P.; Oubre, C.; Prodan, E.; Li, K.; Stockman, M. Plasmon hybridization in nanoparticle dimers. *Nano Lett.* **2004**, *4*, 899–903.

(4) Romero, I.; Aizpurua, J.; Bryant, G. W.; García De Abajo, F. J. Plasmons in nearly touching metallic nanoparticles: singular response in the limit of touching dimers. *Opt. Express* **2006**, *14*, 9988–9999.

(5) Muskens, O. L.; Giannini, V.; Sánchez-Gil, J. A.; Rivas, J. G. Optical scattering res-

onances of single and coupled dimer plasmonic nanoantennas. *Opt. Express* **2007**, *15*, 17736–17746.

(6) Luk'yanchuk, B.; Zheludev, N. I.; Maier, S. A.; Halas, N. J.; Nordlander, P.; Giessen, H.; Chong, C. T. The Fano resonance in plasmonic nanostructures and metamaterials. *Nat. Mater.* **2010**, *9*, 707–715.

(7) Zhang, S.; Genov, D. A.; Wang, Y.; Liu, M.; Zhang, X. Plasmon-Induced Transparency in Metamaterials. *Phys. Rev. Lett.* **2008**, *101*, 047401.

(8) Chiam, S.-Y.; Singh, R.; Rockstuhl, C.; Lederer, F.; Zhang, W.; Bettiol, A. A. Analogue of electromagnetically induced transparency in a terahertz metamaterial. *Phys. Rev. B* **2009**, *80*, 153103.

(9) Liu, N.; Langguth, L.; Weiss, T.; Kästel, J.; Fleischhauer, M.; Pfau, T.; Giessen, H. Plasmonic analogue of electromagnetically induced transparency at the Drude damping limit. *Nat. Mater.* **2009**, *8*, 758–762.

(10) Frimmer, M.; Coenen, T.; Koenderink, A. F. Signature of a Fano Resonance in a Plasmonic Metamolecule's Local Density of Optical States. *Phys. Rev. Lett.* **2012**, *108*, 077404.

(11) Rodriguez, S. R. K.; Murai, S.; Verschuuren, M. A.; Rivas, J. G. Light-Emitting Waveguide-Plasmon Polaritons. *Phys. Rev. Lett.* **2012**, *109*, 166803.

(12) Fleischhauer, M.; Imamoglu, A.; Marangos, J. P. Electromagnetically induced transparency: Optics in coherent media. *Rev. Mod. Phys.* **2005**, *77*, 633–673.

(13) Evlyukhin, A. B.; Bozhevolnyi, S. I.; Pors, A.; Nielsen, M. G.; Radko, I. P.; Willatzen, M.; Albrektsen, O. Detuned electrical dipoles for plasmonic sensing. *Nano Lett.* **2010**, *10*, 4571–4577.

(14) Bozhevolnyi, S. I.; Evlyukhin, A. B.; Pors, A.; Nielsen, M. G.; Willatzen, M.; Albrektsen, O. Optical transparency by detuned electrical dipoles. *New J. Phys.* **2011**, *13*, 023034.

(15) Pors, A.; Willatzen, M.; Albrektsen, O.; Bozhevolnyi, S. I. Detuned electrical dipoles metamaterial with bianisotropic response. *Phys. Rev. B* **2011**, *83*, 245409.

(16) Miroshnichenko, A.; Flach, S.; Kivshar, Y. Fano resonances in nanoscale structures. *Rev. Mod. Phys.* **2010**, *82*, 2257–2298.

(17) Smith, D.; Chang, H.; Fuller, K.; Rosenberger, A.; Boyd, R. Coupled-resonator-induced transparency. *Phys. Rev. A* **2004**, *69*, 063804.

(18) Kekatpure, R.; Barnard, E.; Cai, W.; Brongersma, M. Phase-Coupled Plasmon-Induced Transparency. *Phys. Rev. Lett.* **2010**, *104*, 243902.

(19) Yanik, M.; Suh, W.; Wang, Z.; Fan, S. Stopping Light in a Waveguide with an All-Optical Analog of Electromagnetically Induced Transparency. *Phys. Rev. Lett.* **2004**, *93*, 233903.

(20) Totsuka, K.; Kobayashi, N.; Tomita, M. Slow Light in Coupled-Resonator-Induced Transparency. *Phys. Rev. Lett.* **2007**, *98*, 213904.

(21) Xu, Q.; Sandhu, S.; Povinelli, M.; Shakya, J.; Fan, S.; Lipson, M. Experimental Realization of an On-Chip All-Optical Analogue to Electromagnetically Induced Transparency. *Phys. Rev. Lett.* **2006**, *96*, 123901.

(22) Hicks, E. M.; Zou, S.; Schatz, G. C.; Spears, K. G.; Van Duyne, R. P.; Gunnarsson, L.; Rindzevicius, T.; Kasemo, B.; Käll, M. Controlling plasmon line shapes through diffractive coupling in linear arrays of cylindrical nanoparticles fabricated by electron beam lithography. *Nano Lett.* **2005**, *5*, 1065–1070.

(23) de Abajo, F. J. G.; Sáenz, J. J.; Campillo, I.; Dolado, J. S. Site and lattice resonances in metallic hole arrays. *Opt. Express* **2006**, *14*, 7–18.

(24) García de Abajo, F. J. Colloquium: Light scattering by particle and hole arrays. *Rev. Mod. Phys.* **2007**, *79*, 1267–1290.

(25) Auguié, B.; Barnes, W. Collective Resonances in Gold Nanoparticle Arrays. *Phys. Rev. Lett.* **2008**, *101*, 1–4.

(26) Kravets, V.; Schedin, F.; Grigorenko, a. Extremely Narrow Plasmon Resonances Based on Diffraction Coupling of Localized Plasmons in Arrays of Metallic Nanoparticles. *Phys. Rev. Lett.* **2008**, *101*, 087403.

(27) Vecchi, G.; Giannini, V.; Gómez Rivas, J. Surface modes in plasmonic crystals induced by diffractive coupling of nanoantennas. *Phys. Rev. B* **2009**, *80*, 201401.

(28) Rodriguez, S. R. K.; Abass, A.; Maes, B.; Janssen, O. T. A.; Vecchi, G.; Gómez Rivas, J. Coupling Bright and Dark Plasmonic Lattice Resonances. *Phys. Rev. X* **2011**, *1*, 021019.

(29) Teperik, T. V.; Degiron, A. Design strategies to tailor the narrow plasmon-photonic resonances in arrays of metallic nanoparticles. *Phys. Rev. B* **2012**, *86*, 245425.

(30) Bitzer, A.; Wallauer, J.; Helm, H.; Merbold, H.; Feurer, T.; Walther, M. Lattice modes mediate radiative coupling in metamaterial arrays. *Opt. Express* **2009**, *17*, 758–762.

(31) Ng, B.; Hanham, S. M.; Giannini, V.; Chen, Z. C.; Tang, M.; Liew, Y. F.; Klein, N.; Hong, M. H.; Maier, S. a. Lattice resonances in antenna arrays for liquid sensing in the terahertz regime. *Opt. Express* **2011**, *19*, 14653–14661.

(32) Singh, R.; Rockstuhl, C.; Zhang, W. Strong influence of packing density in terahertz metamaterials. *Appl. Phys. Lett.* **2010**, *97*, 241108.

(33) Schaafsma, M.; Rivas, J. G. Semiconductor plasmonic crystals: active control of THz extinction. *Semicond. Sci. Technol.* **2013**, *28*, 124003.

(34) Humphrey, A. D.; Meinzer, N.; Starkey, T. A.; Barnes, W. L. Surface Lattice Resonances in Plasmonic Arrays of Asymmetric Disc Dimers. *ACS Photonics (in press)*

(35) Sedgwick, F. G.; Pesala, B.; Lin, J.-Y.; Ko, W. S.; Zhao, X.; Chang-Hasnain, C. J. THz-bandwidth tunable slow light in semiconductor optical amplifiers. *Opt. Express* **2007**, *15*, 747–753.

(36) Gan, Q.; Fu, Z.; Ding, Y. J.; Bartoli, F. J. Ultrawide-Bandwidth Slow-Light System Based on THz Plasmonic Graded Metallic Grating Structures. *Phys. Rev. Lett.* **2008**, *100*, 256803.

(37) Zhang, J.; Cai, L.; Bai, W.; Xu, Y.; Song, G. Slow light at terahertz frequencies in surface plasmon polariton assisted grating waveguide. *J. Appl. Phys.* **2009**, *106*, –.

(38) Bai, Q.; Liu, C.; Chen, J.; Cheng, C.; Kang, M.; Wang, H.-T. Tunable slow light in semiconductor metamaterial in a broad terahertz regime. *J. Appl. Phys.* **2010**, *107*, –.

(39) Gu, J.; Singh, R.; Liu, X.; Ma, Y.; Zhang, M.-S. A., Shuang; Tian, Z.; Azad, A. K.; Chen, H.-T.; Taylor, A. J.; Han, Z.-W., Jiaguang Active control of electromagnetically induced transparency analogue in terahertz metamaterials. *Nat. Commun.* **2012**, *3*, 1151.

(40) Novotny, L. Effective Wavelength Scaling for Optical Antennas. *Phys. Rev. Lett.* **2007**, *98*, 266802.

(41) Rivas, J. G.; Benet, A. F.; Niehusmann, J.; Bolivar, P. H.; Kurz, H. Time-resolved broadband analysis of slow-light propagation and superluminal transmission of electromagnetic waves in three-dimensional photonic crystals. *Phys. Rev. B* **2005**, *71*, 155110.

(42) Zentgraf, T.; Zhang, S.; Oulton, R. F.; Zhang, X. Ultranarrow coupling-induced transparency bands in hybrid plasmonic systems. *Phys. Rev. B* **2009**, *80*, 195415.

(43) Jensen, T.; Kelly, L.; Lazarides, A.; Schatz, G. C. Electrodynamics of Noble Metal Nanoparticles and Nanoparticle Clusters. *J. Cluster Sci.* **1999**, *10*, 295–317.

(44) De Abajo, F. G.; Sáenz, J. Electromagnetic surface modes in structured perfect-conductor surfaces. *Phys. Rev. Lett.* **2005**, *95*, 233901.

(45) Zou, S.; Schatz, G. C. Narrow plasmonic/photonic extinction and scattering line shapes for one and two dimensional silver nanoparticle arrays. *J. Chem. Phys.* **2004**, *121*, 12606–12612.

(46) van de Hulst, H. C. *Light Scattering by small particles*; Dover Publications, Inc., 1981.

Graphical TOC Entry

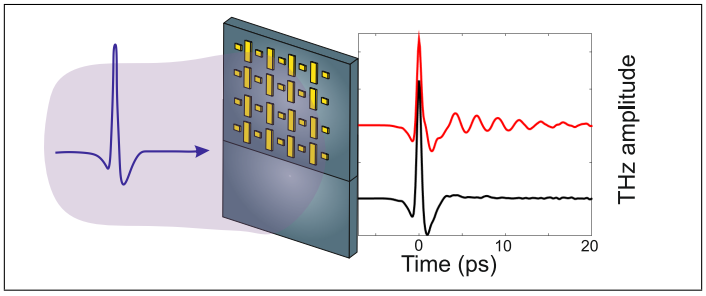

For Table of Contents Use Only

Diffraction enhanced transparency and slow THz light in periodic arrays of detuned and displaced dipoles by M. C. Schaafsma, A. Bhattacharya and J. G. Rivas

We demonstrate that a periodic lattice of detuned resonators can suppress the THz extinction at the central resonant frequency, leading to diffraction enhanced transparency (DET). The system consists of metallic rods of two different sizes, each of them supporting a strong half-wavelength ($\lambda/2$) resonance, which are spatially displaced within the unit cell of the lattice. Using a coupled dipole model we show that the DET window has its origin in the interference between two surface lattice resonances, arising from the diffractively enhanced radiative coupling of the $\lambda/2$ resonances in the lattice. Group-index measurements show that the THz field is strongly delayed by more than four orders of magnitude at the transparency window. Since DET does not involve the near-field coupling of resonators, the fabrication tolerance to imperfections is expected to be very high. This remarkable response renders these systems as very interesting components for THz communication.